Characteristics of nighttime medium-scale traveling ionospheric disturbances observed over Alaska

Minoru Kubota,[1] Mark Conde,[2] Mamoru Ishii,[1] Yasuhiro Murayama,[1] and Hidekatsu Jin[1]

Received 14 October 2010; revised 4 February 2011; accepted 9 February 2011; published 10 May 2011.

[1] We focused on propagating wave-like structures which frequently appeared in the O I 630.0 nm airglow images obtained by an all-sky imager installed at Poker Flat Research Range (65.1°N, 147.4°W, magnetic latitude 65.6°) in Alaska. These events are classified as medium-scale traveling ionospheric disturbances (MSTIDs) on the basis of the wavelength and propagating speed. The unique points of our observation are (1) the two-dimensional structures of MSTIDs in the subauroral region are revealed; (2) the horizontal direction of the electric field can be estimated from the motion of the Evening Co-rotating Patch (ECP) aurora appearing simultaneously; and (3) neutral winds are simultaneously observed by a Fabry-Perot spectrometer. Statistical study of these MSTID events from November 2001 to April 2002 indicates the following characteristics. The MSTIDs were observed almost every evening, and sometimes in the morning, but were not observed at midnight. Typical propagating speed, direction, and wavelength of the wave phenomena were about 135 m/s, southwestward, and about 250 km, respectively. When the MSTIDs appeared, northward neutral winds and westward plasma drifts were dominant. This indicates that the Perkins instability does not contribute to the development of MSTIDs in the Alaska region. The vertical wavelength analysis using the dispersion relation of gravity waves with the observed wave parameters and background winds suggests that the observed MSTIDs over Alaska are the atmospheric gravity waves (AGWs). As a case study, temporal variation of an MSTID event on 21 December 2001 is shown. Results of a ray tracing analysis of this event suggest that the AGWs come from the equatorward edge of the auroral oval.

Citation: Kubota, M., M. Conde, M. Ishii, Y. Murayama, and H. Jin (2011), Characteristics of nighttime medium-scale traveling ionospheric disturbances observed over Alaska, *J. Geophys. Res.*, *116*, A05307, doi:10.1029/2010JA016212.

1. Introduction

[2] We frequently observe periodic ionospheric fluctuations called traveling ionospheric disturbances (TIDs). *Hunsucker* [1982] reviewed theoretical and observational results describing AGW or TID phenomena, and classified TIDs into three types: large-scale TIDs, medium-scale TIDs (MSTIDs), and small-scale TIDs. According to his classification, MSTIDs have horizontal wavelength and period of several hundred kilometers and 15–60 min, respectively.

[3] MSTIDs appear to be present in all geographic locations. Many investigations have been carried out especially in the midlatitude region. *Kubota et al.* [2000] showed that MSTIDs traveled a horizontal distance of more than 1000 km, and lasted for more than 3 h using a multipoint network of all-sky imagers (ASIs) over Japan. *Saito et al.* [1998] first showed two-dimensional maps of TEC perturbations caused by MSTIDs over Japan using a dense GPS network consisting of about 1,000 GPS receivers. *Shiokawa et al.* [2003a] showed that most MSTIDs observed at night over Japan propagate southwestward in all seasons. Using a GPS receiver network in Southern California, *Kotake et al.* [2007] found that the characteristics of MSTIDs differ during the day, at dusk, and during the night. An electric force resulted from the electric field perturbation, which could be caused by plasma instability, is one possible source of MSTIDs [e.g., *Perkins*, 1973]. *Shiokawa et al.* [2003b] showed an electric field perturbation accompanied by an MSTID structure in a midlatitude region using simultaneous observation of an all-sky imager and DMSP satellite. *Otsuka et al.* [2004] conducted observations of MSTIDs at Sata, Japan and Darwin, Australia. They observed MSTID structures conjugate in the northern and southern hemisphere, connected by geomagnetic field lines. This result indicates that polarization electric fields play an important role in the generation of MSTIDs in the midlatitude region.

[4] In the high-latitude region, *Oyama et al.* [2001] investigated the relationship between auroral activities and neutral wind oscillations in the polar *F* region observed by EISCAT radar. Their results suggest that high-latitude geomagnetic activity is an important source of AGWs or TIDs. The

[1]National Institute of Information and Communications Technology, Tokyo, Japan.
[2]Geophysical Institute, University of Alaska Fairbanks, Fairbanks, Alaska, USA.

0148-0227/11/2010JA016212

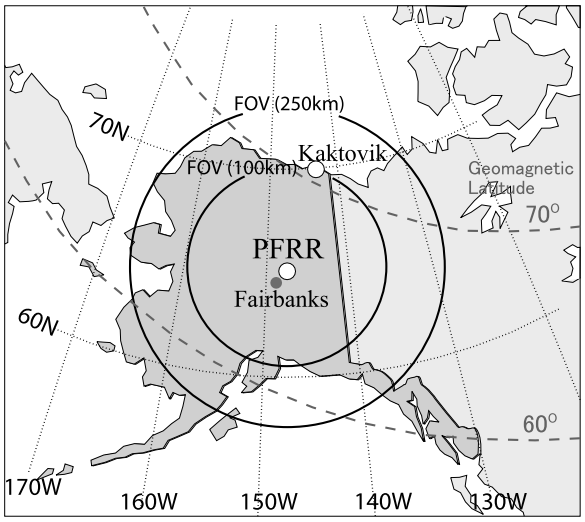

Figure 1. Map of an area around Alaska, with the location of the observation site, PFRR. Two circles show the observational FOVs when the airglow emission altitudes are assumed to be 100 and 250 km. The dashed lines represent the magnetic latitudes of 60° and 70°.

SuperDARN HF radar network is a powerful tool for observing AGWs or TIDs in high-latitude regions [*Samson et al.*, 1989]. The AGW or TID signature in the HF radar data is a quasiperiodic enhancement of the ground-backscattered power that propagates away from its source region. *Bristow et al.* [1996] investigated the seasonal dependence of the AGWs or TIDs observed by the SuperDARN. They showed a higher probability of observing an AGW or TID during winter than during summer, and suggested that the lower probability of an AGW in summer is caused by AGW reflection from the temperature gradient associated with the cold summer mesosphere. It should be noted that the ground backscatter echoes are generally observed during the day. Therefore, nighttime observations of MSTIDs in high-latitude regions are insufficient.

[5] The O I 630 nm nightglow can be an important indicator of thermospheric and ionospheric disturbances [*Barbier*, 1959; *Barbier and Glaume*, 1962]. All-sky imaging observation of the O I 630 nm emission intensity reveals the behavior of the MSTIDs in detail [e.g., *Kubota et al.*, 2001].

[6] At high latitudes, MSTID observations using ASI have been thought to be difficult, because of the presence of the bright aurora hindering detection. Nevertheless, we found that the MSTID structures often appear in the O I 630 nm images obtained by the ASI installed at Poker Flat Research Range in Alaska. In this paper, the characteristics of the nighttime MSTID in the subauroral region are identified, and the source of the MSTIDs is discussed.

2. Observations

[7] We used two all-sky imagers (ASIs) developed by National Institute of Information and Communications Technology (NICT) [*Kubota et al.*, 2002]. The ASI consists of a fisheye lens, telecentric lens system, filter turret, bare CCD camera controlled by personal computer. The ASI covers a 180° field of view (FOV), which means it can observe airglow emissions over the whole sky, from zenith to horizon. The sensitivity of these imagers and the non-uniformity in their image planes were calibrated using an integrating sphere facility. *Yamamoto et al.* [2002] described techniques for obtaining absolute intensity distributions of aurora/airglow emissions from the ASI observation data.

[8] The two ASIs were installed at Poker Flat Research Range (PFRR) (65.1°N, 147.4°W, magnetic latitude 65.6°) of the University of Alaska Fairbanks, and observations commenced in October 2000. Figure 1 shows the effective FOVs of these ASIs assuming two different emission heights. This system was operated automatically and fully controlled from NICT in Japan. Observation data were automatically sent to NICT via the System for Alaska Middle Atmosphere Observation Data Network (SALMON) [*Oyama et al.*, 2002], and summarized data are available to the public online at http://salmon.nict.go.jp/.

[9] This study used ASI data obtained from November 2001 to April 2002. During this period, O I 630.0 nm and O I 557.7 nm emission images were obtained every 5 min with exposure times of 5 s and 3 s, respectively. In the data analysis, we used horizontal neutral wind velocities in the *F* region observed by the Scanning Doppler Imager (SDI) installed at PFRR. The SDI is an all-sky imaging Fabry-Perot spectrometer which can observe two-dimensional distributions of thermospheric neutral winds. This study used zonal and meridional wind velocities derived with an assumption of uniform wind over the whole sky as background winds. The SDI system is described in detail by *Conde and Smith* [1997, 1998].

3. Observational Results

[10] In the ASI observations at PFRR, wave-like structures were often observed in the O I 630.0 nm emission. This chapter shows the characteristics of these phenomena derived from a case study and statistical study in sections 3.1 and 3.2, respectively.

3.1. Case Study (21 December 2001)

[11] On 21 December 2001, ASI data collection started after sunset at approximately 0200 UT, and stopped at sunrise at approximately 1730 UT. The sky was clear on this night, with Moon at low elevation angles until 0500 UT, and moderate auroral breakups occurred from midnight to morning. Figure 2 shows typical images of O I 557.7 and O I 630.0 nm on this night. In the O I 557.7 nm image (left panel), irregularly shaped spots are seen; these are the Evening Co-rotating Patch (ECP) aurora [*Kubota et al.*, 2003]. In the O I 630.0 nm image (right panel), which is an intensity deviation from an image averaged over 1 h, a wave structure consisting of a few stripes extending from southeast to northwest appears. A movie of the O I 557.7 and O I 630.0 nm data is available in Animation S1.[1] The movie includes strong evidence that the wave structure propagates southwestward from 0230 to 0530 UT. Because the relationship between local time (LT) at PFRR and universal time (UT) is given by LT = UT − 10 h, the wave

[1] Auxiliary materials are available in the HTML. doi:10.1029/2010JA016212.

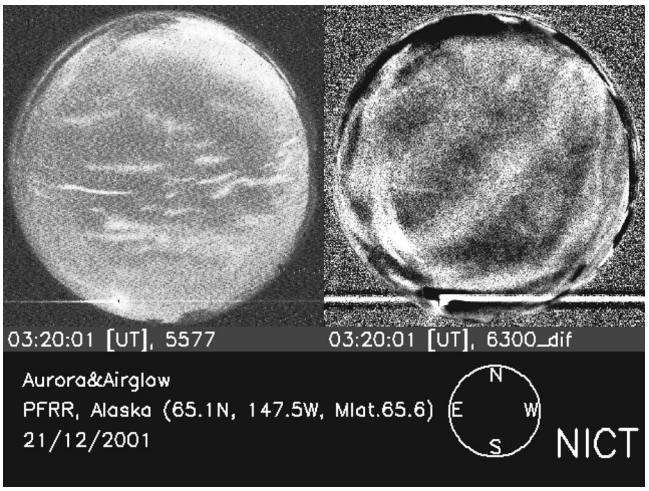

Figure 2. (left) All-sky image of O I 557.7 nm emission at 0240 UT on 21 December 2001. The gray scale shows the emission intensity in arbitrary units. (right) O I 630.0 nm emission image at the same time. The gray scale shows the intensity deviation from a 1 h average. The bright dots and horizontal lines near the southern edge of the images are caused by the Moon.

structure appearance time is equivalent to 1630–1930 LT on the evening of the preceding day.

[12] Figure 3 (top) shows two-dimensional distributions of O I 630.0 nm emissions intensity projected on the map of Alaska and Yukon. In the northeast part of these images, we can see the low-latitude edge of the auroral oval. The aurora emission intensity in this region rose quickly between 0320 UT and 0405 UT. Figure 3 (bottom) shows intensity deviations from an image averaged over 1 h. A wavefront can be seen in the lower-latitude region of the auroral oval. The black dashed line shows a wave structure propagating southwestward with a velocity of 185 m/s. This phase velocity is obtained manually from the sequential images in Figure 3. The wavefront is parallel to the auroral oval and indicates that the wave is propagating toward geomagnetic south. Another wave structure is indicated by the white dashed lines. The inclination of its wavefront, which looks like part of a circular arc, is slightly different from the first wave, and the propagating direction of the second wave is west-southwestward with a velocity of 105 m/s. Animation S2 shows a movie of the map-projected O I 630.0 nm emissions during 0240 UT and 0530 UT. The wave structure parallel to the auroral oval appears at 0330 UT and seems to continue until 0530 UT. Another wave structure which looks like part of a circular arc appears before 0230 UT and seems to continue until 0400 UT.

[13] Variations of airglow and aurora emission intensities, the ground geomagnetic field *H* component at PFRR and Kaktovik (70.1N, 143.6W), and thermospheric neutral wind are compiled in Figure 4. Figures 4a and 4b show the high-pass filtered, S-N and W-E keograms of the O I 630.0 nm emission intensity, respectively. The filter period is 1 h. Wave-like structures became visible as a result of the filtering process. To confirm that these wave-like structures are not due to clouds, we made filtered keograms of the O I 557.7 nm emission with the same procedure. The MSTID-like structures could not be seen in the O I 557.7 nm keograms (not shown). In Figures 4a and 4b, the wave structures appear near the observation start time at 0200 UT and continue until about 0600 UT. Variations of the emission intensity from this wave exceed 5% at the beginning and decrease with duration. The bright auroral 630.0 nm enhancements are masked by black color. After 0600 UT, auroral activity increase and the wave structures are missing. Because multiple waves are superimposed, wave structures appearing in Figure 4 are slightly irregular. However, this pattern indicates that the propagation direction of the wave was approximately southwestward. The southward and westward propagating velocities of the wave structures can be measured manually from their slopes. Based on Figure 4, the horizontal phase velocities of the wavefront are estimated at 75–190 m/s, and this is consistent with the phase velocities derived from Figure 3. A period of fluctuation derived from the gap of wave structures is about 30 min. The horizontal wavelengths calculated from the phase velocities and the periods were about 135–340 km. From the phase velocity, period, and wavelength, the wave features are classified as MSTIDs [*Hunsucker*, 1982].

[14] Keograms of the O I 557.7 nm emission intensity in Figures 4c and 4d indicate the appearance of ECP aurora between 0200 UT and 0400 UT, which appear here as white filaments. In the S-N keogram (Figure 4c), the ECP aurora appears near the zenith and slightly drifts southward. In the W-E keogram (Figure 4d), it drifts westward. This indicates that the plasma drift direction, which coincides with the direction of the aurora patch drift [e.g., *Kubota et al.*, 2003], is west-southwestward. Geomagnetic activity at PFRR shown in Figure 4e is quiet until 0600 UT and moderately disturbed after that. This is consistent with the auroral activity, which increases after 0600 UT above PFRR, as shown in Figures 4c and 4d. Variations of thermospheric neutral winds in Figures 4f and 4g indicate a northwestward or northward wind direction during the MSTID existence. The characteristics of the MSTID derived from the observational results are schematically illustrated in Figure 5.

3.2. Statistical Study

[15] We investigated the statistical characteristics of the MSTID observed in the O I 630.0 nm airglow images at PFRR using data obtained from November 2001 to April 2002. During this period, airglow/aurora images on 44 nights with clear sky conditions could be obtained. Observation data are divided into 30 min bins. The bins during the aurora enhancements are excluded. As a result, 320 bins with clear sky and no aurora were obtained. For each bin, the MSTID occurrence, propagating direction, phase velocity, period, wavelength, background neutral wind velocity, direction, and plasma drift direction were investigated. When the MSTIDs appeared, their phase velocities and propagating directions were measured manually from the slopes of the wave structures in the high-pass filtered S-N and W-E keograms of the O I 630.0 nm emission intensity. The periods were derived from the gap of the wave structures. The wavelengths were calculated by the phase velocities and periods. The background neutral wind velocities and directions were obtained by the SDI system. The plasma drift directions were derived from the motions of the ECP aurora

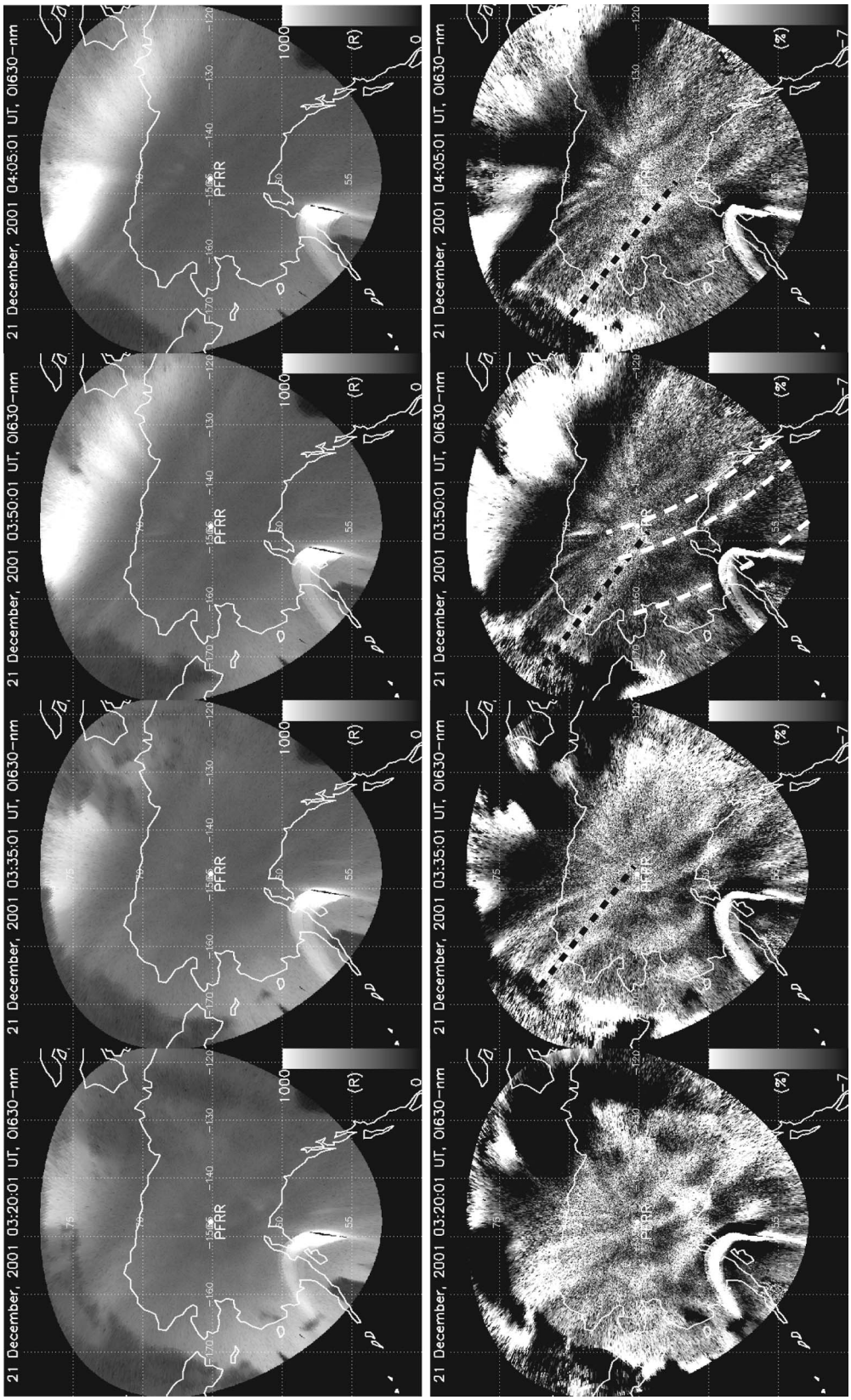

Figure 3. Two-dimensional maps of the O I 630.0 nm emission intensity from 0320 to 0405 UT, every 15 min. Gray scales show (top) the absolute intensity and (bottom) the intensity deviations from the 1 h average. The black dashed line indicates a wavefront parallel to the auroral oval and propagating toward geomagnetic south. The white dashed lines indicate another wave structure which looks like part of a circular arc.

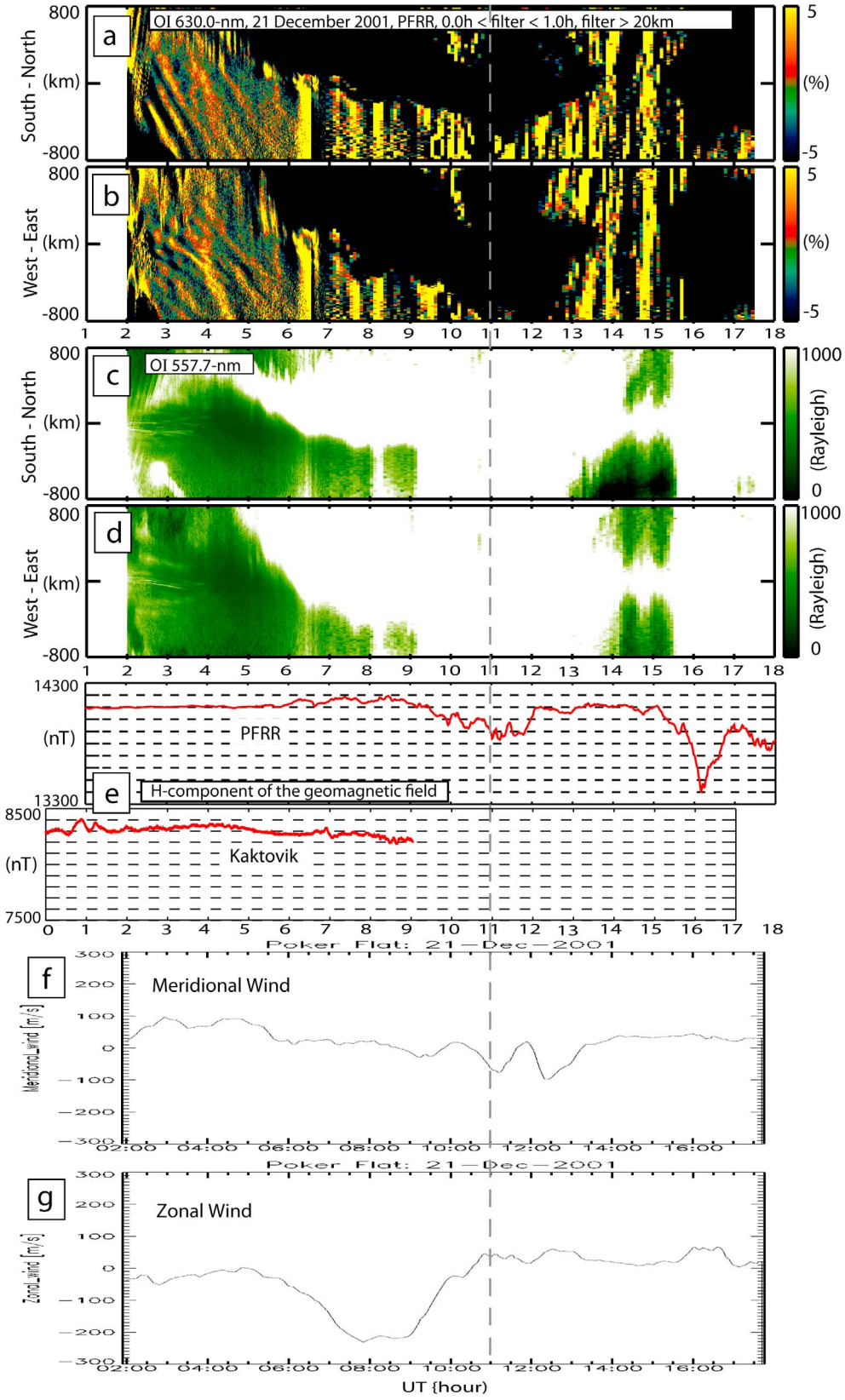
a
OI 630.0-nm, 21 December 2001, PFRR, 0.0h < filter < 1.0h, filter > 20km
South - North
(km)
800
-800
5
(%)
-5
b
West - East
c
OI 557.7-nm
1000
(Rayleigh)
0
d
1 2 3 4 5 6 7 8 9 10 11 12 13 14 15 16 17 18
14300
(nT)
PFRR
13300
e
H-component of the geomagnetic field
8500
Kaktovik
7500
Poker Flat: 21-Dec-2001
f
Meridional Wind
Meridional wind [m/s]
300
200
100
0
-100
-200
-300
02:00 04:00 06:00 08:00 10:00 12:00 14:00 16:00
g
Zonal Wind
Zonal wind [m/s]
UT (hour)

Figure 4

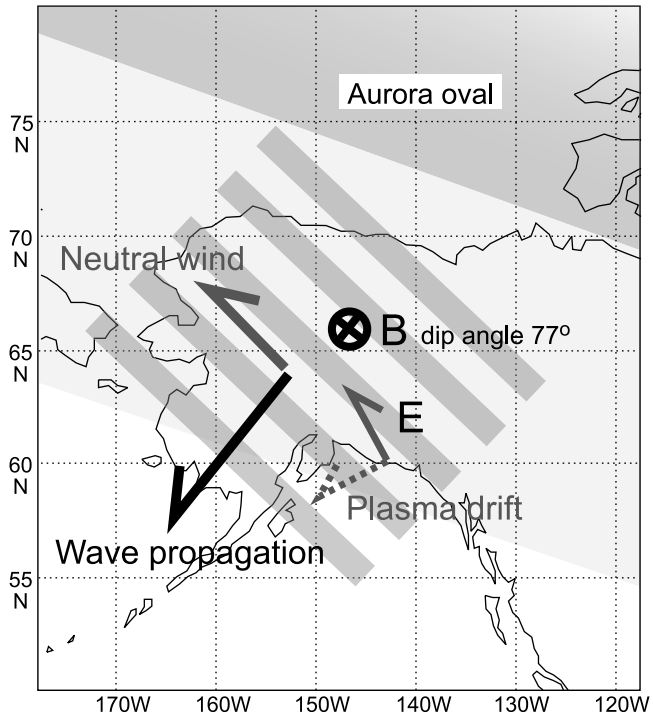

Figure 5. Schematic view of the MSTID, plasma drift, and neutral wind observed at PFRR in the evening of 21 December 2001.

which appeared in keograms of the O I 557.7 nm emission intensity.

[16] Figure 6 (left) is a histogram of these bins for the entire period, and shows the relationship between MSTID occurrence and local time. The number of bins from midnight to morning is much lower than in the evening, because auroral activity in Alaska is generally high from midnight to morning. The total number of bins before 20 LT is 160. Of this, MSTIDs were observed in 90% (145 bins). MSTIDs could not be observed in the middle of the night, and few were observed in the morning. This indicates that the occurrence rate of MSTIDs is larger in the evening than in the middle of the night or the morning. Figure 6 (right) shows monthly histograms from November 2001 to April 2002. The time of occurrence of the MSTIDs varies from month to month, and seems to depend on the time of sunset and sunrise.

[17] Figure 7 shows histograms of the MSTID period (Figure 7a), phase velocity (Figure 7b), and wavelength (Figure 7c). Their respective mean values are 33 min, 134 m/s, and 263 km. Figure 7d shows the MSTID propagation direction, indicating that southwestward is dominant. Figure 8 shows (Figure 8a) background neutral wind direction observed by SDI when MSTIDs appear (on) and when they are not observed (off) and (Figure 8b) plasma drift direction obtained from the motions of the ECP aurora. Background neutral wind direction is generally northward, and north-northwestward wind is dominant. On the other hand, for the plasma drift, west-southwestward drift is dominant. The dominant direction of the electric field estimated from the plasma drift direction is north-northwestward.

4. Discussion

[18] Wavelength, phase velocity, and propagation direction (southwestward) of MSTIDs above Alaska are very similar to those of MSTIDs observed in midlatitude regions [e.g., *Kubota et al.*, 2000; *Shiokawa et al.*, 2003a]. *Shiokawa et al.* [2003b] suggested that the amplitudes of airglow intensity variation over Japan cannot be explained by the gravity wave, and that the polarization electric field plays an important role in MSTID generation. The Perkins instability plays an important role in developing MSTIDs in midlatitude regions. In the Alaska region, by contrast, it is unlikely that Perkins instability would contribute to the development of MSTIDs, because it can only be maintained by an eastward electric field or equatorward wind [*Perkins*, 1973; *Huang et al.*, 1994]. We therefore assume that MSTIDs in this region are caused solely by atmospheric gravity waves (AGW), and verify this through observations.

[19] The vertical wavelength of the gravity wave (λ_z) can be estimated from wave period (T), zonal and meridional phase velocities (v_{px} and v_{py}) and background neutral wind using the dispersion relationship, which can be written as follows [e.g., *Kubota et al.*, 2006; *Marks and Eckermann*, 1995]:

$$\frac{(2\pi)^2}{\lambda_z^2} = m^2 = \frac{(k^2+l^2)(N^2-\omega_{\mathrm{int}}^2)}{\omega_{\mathrm{int}}^2 - f^2} - \frac{1}{4H^2}$$
$$k = 2\pi/(v_{px}\mathrm{T}) \qquad , \qquad (1)$$
$$l = 2\pi/(v_{py}\mathrm{T})$$

where ω_{int} is the intrinsic frequency of the gravity wave, f is the inertial frequency, N is the Brunt–Väisälä frequency, H is the scale height, and k, l, and m are zonal, meridional, and vertical wave numbers, respectively. We obtained the values of N and H by using the MSISE-90 model [*Hedin*, 1991]. The intrinsic frequency is related to the observed frequency by

$$\omega_{\mathrm{int}} = \omega - kU - lV - mW \qquad ,$$
$$\omega = 2\pi/\mathrm{T}$$

Figure 4. (a) High-pass filtered S-N keogram of the O I 630.0 nm emission intensity. The filter period is 1 h. The vertical axis indicates the northward distance from the zenith. The dashed gray vertical line indicates the magnetic midnight. (b) Same type of section as Figure 4a but for the W-E keogram and eastward distance from the zenith. (c) Keogram of the O I 557.7 nm emission intensity. The vertical axis indicates the northward distance from the zenith. (d) Same type of section as Figure 4c but for the eastward distance from the zenith. (e) Variation of the H component of the geomagnetic field observed at PFRR and Kaktovik. (f) Meridional neutral wind in the F region measured by the SDI. (g) Same as Figure 4f but for the zonal neutral wind.

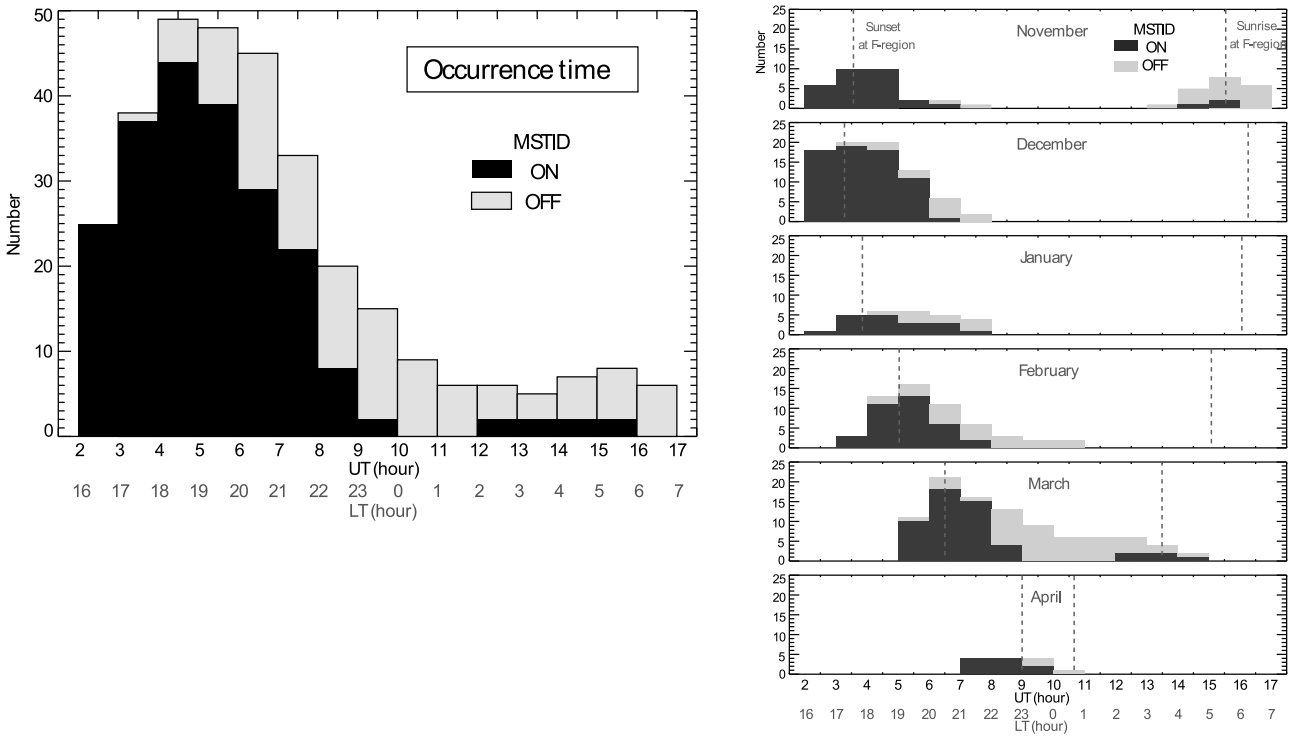

Figure 6. (left) Histogram showing the relationship between MSTID occurrence and time. (right) Monthly histograms from November 2001 to April 2002.

where ω is the ground-based wave frequency, U, V, and W are background wind velocities in the zonal, meridional, and vertical directions, respectively.

[20] Figure 9 shows a variation of the vertical wavelength of the MSTID in the case study on 21 December 2001. In the calculation of the vertical wavelength, we assigned values of 100 and 200 m/s as v_{px} and v_{py}, respectively, which are read from keograms shown in Figures 4a and 4b. We also assumed that $W = 0$, and v_{px}, v_{py}, k, l, and ω were constant through the night. Wind velocities in the F region measured by the SDI are used as the background neutral wind velocities. On this night, the vertical wavelength was about 100 km at around 03 UT. After 04 UT, the vertical wavelength decreased and reached a critical level (~0) at about 07 UT. On the other hand, the wave structures in Figure 4a were clearly visible before 04 UT. These structures were then reduced in amplitude and disappeared after 06UT. The variation of the vertical wavelength shown in Figure 9 is consistent with the variation of the amplitude of intensity fluctuation observed by ASI from the ground. This suggests that the MSTID above Alaska has the properties of the AGW.

[21] One important characteristic of the MSTID above Alaska is that it mostly propagates southwestward. Three possible reasons have been identified as follows.

[22] 1. The first reason is the filtering effect by the neutral wind. When phase velocity of the AGW is comparable to the background wind velocity in the same direction, the vertical wavelength of the gravity wave (λ_z) decreases. When λ_z is much smaller than the thickness of the O I 630.0 nm emission layer, the wave structures observed from the ground are reduced in amplitude and disappear. When λ_z reaches a critical level (~0), the AGW dissipates then and there, and cannot propagate to higher altitudes. Figure 10 shows histograms of vertical wavelengths estimated for the 320-bin data set used in the statistical study (Figure 10a) when the MSTIDs appear (on) and (Figure 10b) when they are not observed (off). The vertical wavelengths were calculated from equation (1) based on the estimated values of wave period (T), zonal and meridional phase velocities (v_{px} and v_{py}), and measured background neutral winds for each bin. When MSTIDs were not observed we assigned values of 30 min, 150, and 200 m/s as T, v_{px}, and v_{py}, respectively, which are the median values in the entire period. In Figure 10, the vertical wavelengths from 50 km to 500 km are dominant when the MSTIDs appear, and the vertical wavelengths less than 100 km or evanescent cases are dominant when MSTIDs are not observed. This result suggests that the filtering effect by the neutral wind plays a certain role in determining the MSTID propagating direction.

[23] 2. The second reason is the effect created by the relationship between the wave pattern and inclination of the geomagnetic field line. Previous studies [*Hooke*, 1970; *Kotake et al.*, 2007] suggest that equatorward propagating gravity waves could cause the amplitude of TEC perturbations to be larger than would result from gravity waves propagating in other directions. Ions in the F region move along the geomagnetic field lines through neutral ion collisions. *Hooke* [1968] showed that the velocity of the ion motion along the geomagnetic field is the same as that of theneutral motion along the geomagnetic field caused by gravity waves. However, the ion motion across the magnetic field line (**B**) is restricted because the ion gyrofrequency is much higher than the ion-neutral collision frequency. This

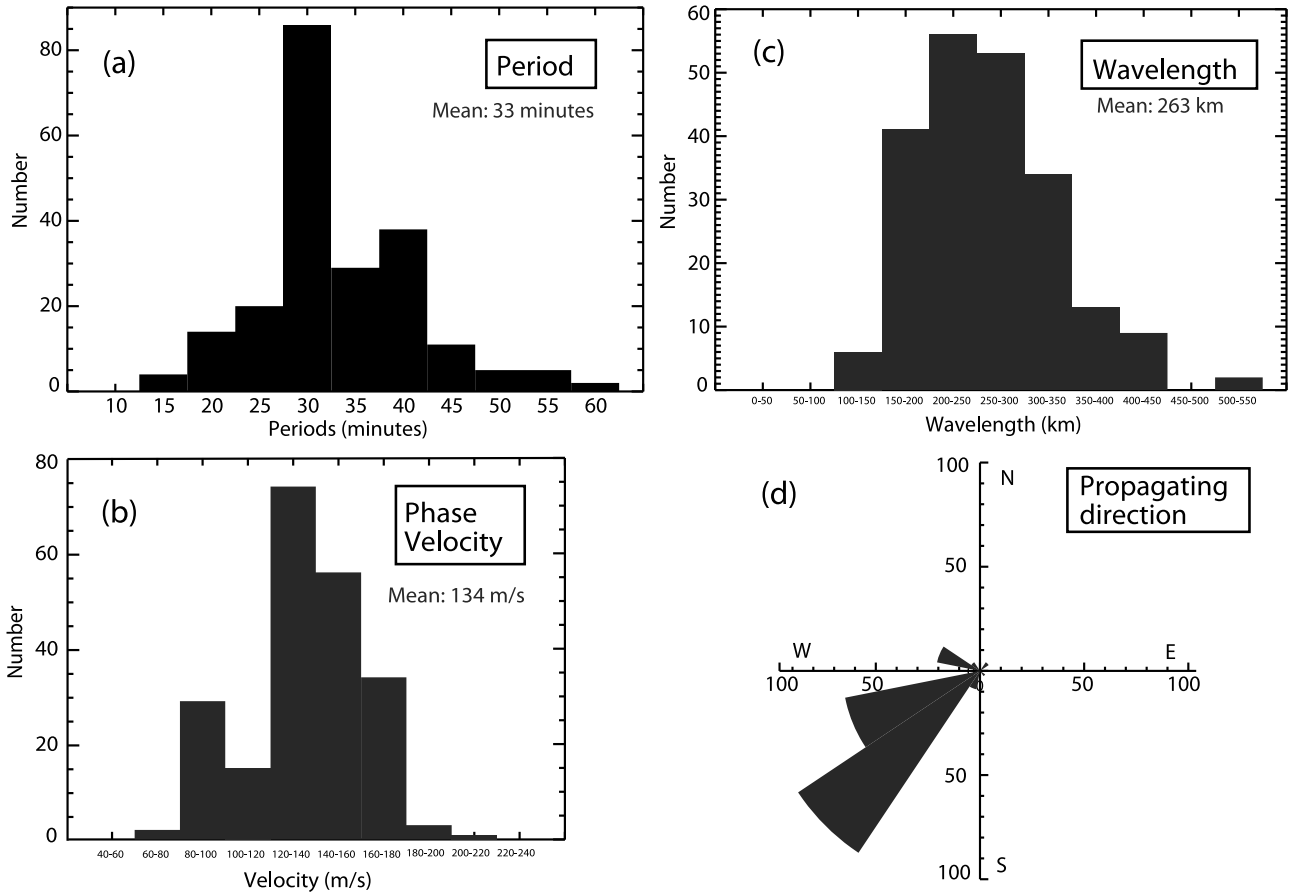

Figure 7. Histograms of (a) period, (b) phase velocity, (c) wavelength, and (d) propagating direction of MSTIDs.

directivity of the ion mobility produces the directivity in the response of the electron density variations to the neutral motion caused by gravity waves. Such directivity in response to the *F* region plasma of gravity waves could be responsible for the magnetic southward preference in the propagation directions of the MSTID.

[24] 3. The third reason is the location of the major wave source. There are some reports of gravity waves generated by the Joule or particle heating in the auroral oval [e.g., *Kubota et al.*, 2000; *Oyama et al.*, 2001; *Francis*, 1974]. During the day and early at night, the auroral oval is usually located northeastward of Alaska, as shown in Figure 3. The MSTIDs from the auroral oval should propagate southwestward over Alaska. Two MSTIDs observed on 21 December 2001 have different features. The wavefront of AGW "A," indicated by the black dashed line in Figure 3, is straight and parallel to the auroral oval. This shape of the wavefront suggests that the wave source has long and straight configuration. The wavefront of AGW "B," indicated by the white dashed lines in Figure 3, has a curved structure. This suggests that the wave comes from a point source, or a curved configuration of current.

[25] As the next step in the data analysis, we applied a ray tracing technique to investigate the source of the MSTID. We used the ray tracing equations described by *Marks and Eckermann* [1995] to trace backward the trajectory of the AGW from an altitude of 250 km to an altitude of 100 km. The equations can be written as follows:

$$C_{gx} = \frac{dx}{dt} = U + \frac{k\left(N^2 - \omega_{\text{int}}^2\right)}{\omega_{\text{int}}\Delta}$$

$$C_{gy} = \frac{dy}{dt} = V + \frac{l\left(N^2 - \omega_{\text{int}}^2\right)}{\omega_{\text{int}}\Delta}$$

$$C_{gz} = \frac{dz}{dt} = \frac{-m\left(\omega_{\text{int}}^2 - f^2\right)}{\omega_{\text{int}}\Delta}$$

$$\Delta = k^2 + l^2 + m^2 + \alpha^2\ , \quad \alpha = \frac{1}{4H^2}$$

$$\frac{dk}{dt} = 0$$

$$\frac{dl}{dt} = \frac{-f \cdot f_y(m^2 + \alpha^2)}{\omega_{\text{int}}\,\Delta}\ , \quad f_y = \frac{df}{dy}$$

$$\frac{dm}{dt} = -k\frac{dU}{dz} - l\frac{dV}{dz} - \frac{N_z^2\,(k^2 + l^2) - \alpha_z^2\left(\omega_{\text{int}}^2 - f^2\right)}{2\omega_{\text{int}}\Delta},$$

$$N_z^2 = \frac{dN^2}{dz}\ , \quad \alpha_z^2 = \frac{d\alpha^2}{dz}$$

where C_{gx}, C_{gy}, and C_{gz} are zonal, meridional, and vertical group velocities of the AGW, respectively. To obtain the values of the Brunt-Väisälä frequency (N) and the scale height (H), we used the MSISE-90 model [*Hedin*, 1991].

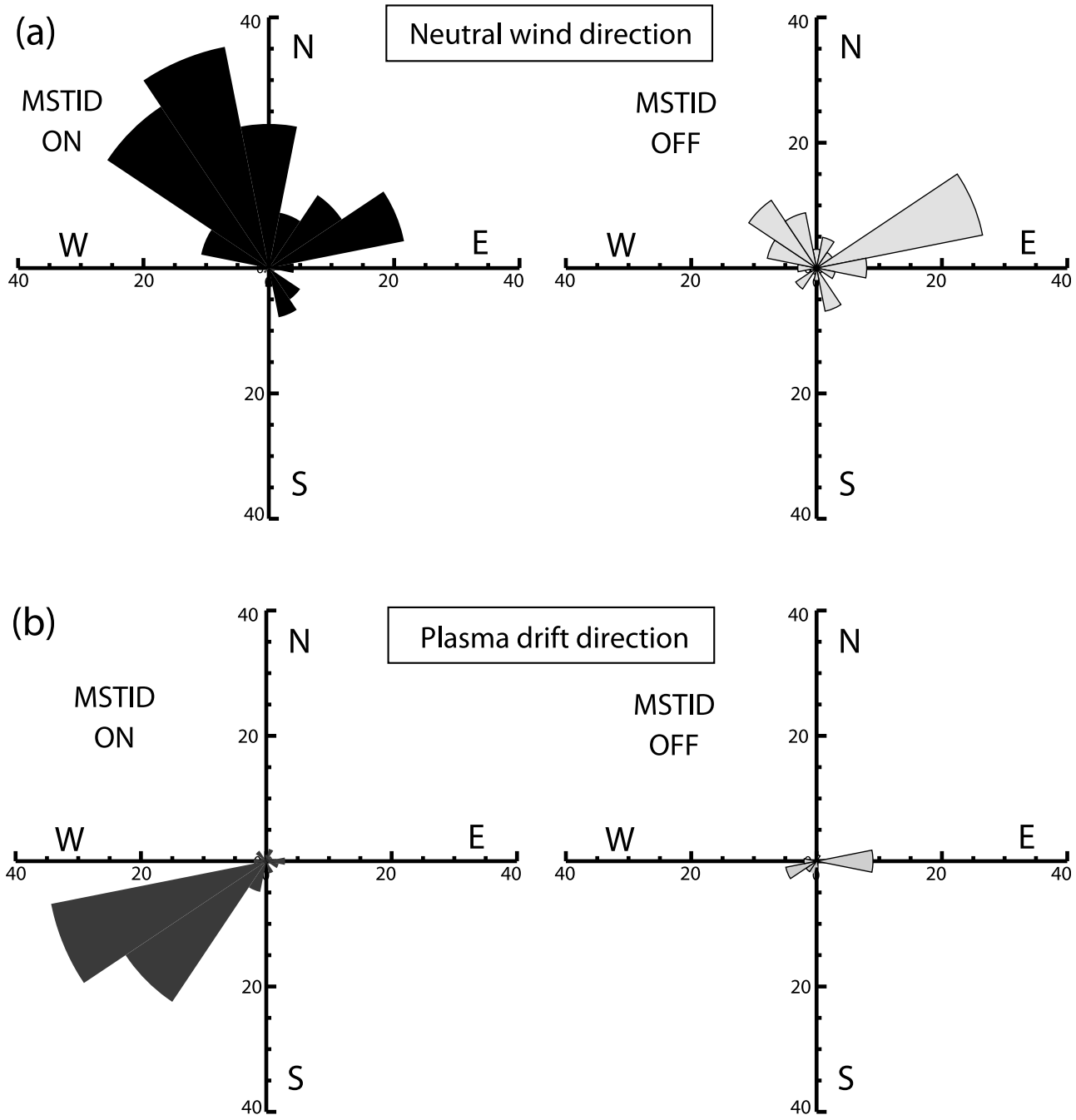

Figure 8. (a) Relationship between background wind direction and MSTID occurrence. (b) Relationship between plasma drift direction and MSTID occurrence.

The background wind velocities (U and V) were obtained from the horizontal wind model (HWM) [*Hedin et al.*, 1996]. These data (U, V, N, and H) were linearly interpolated to obtain a data set with 100 m height resolution. In the calculation, we used a time step of 100 m/C_{gz}, where 100 m was a height increment. Figure 11 shows the ray tracing results for the two MSTIDs shown in Figure 3. Wave "A" indicated by a black dashed line in Figure 3 traced northeastward, and reached the lower-latitude edge of the auroral oval at 100 km altitude, as shown in Figure 11a. Wave "B" indicated by white dashed lines in Figure 3 traced east-northeastward, and reached another point of the lower-latitude edge of the auroral oval at 100 km altitude, as shown in Figure 11b. The time taken for the wave propagation from 100 km to 250 km was estimated at about 3 h. The horizontal wind velocity derived from the model could cause a calculation error in the ray tracing. To examine the extent of the error, we also calculated the backward trajectory of the AGW with an assumption of $U = V = 0$. The results of the calculation are shown in Figure 11 with gray lines. The directions of the raypaths were almost identical in the two cases, and the difference in the traced point was not very significant in this study. These results suggest that the MSTIDs observed from PFRR are generated near the

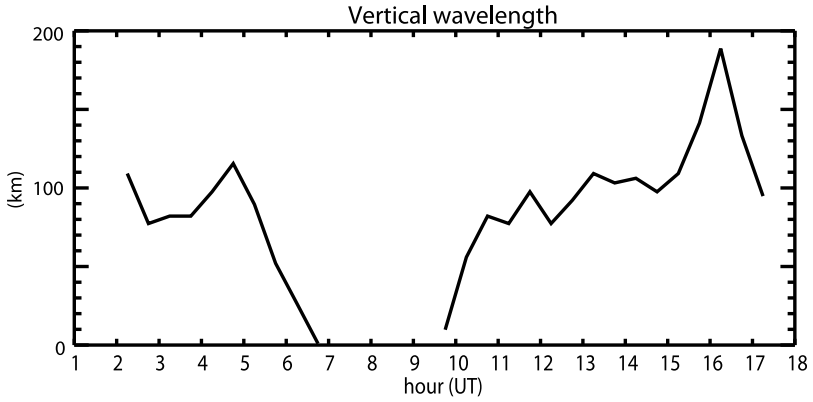

Figure 9. Variation of the vertical wavelength of the MSTID estimated using neutral wind velocities in the case study on 21 December 2001.

lower-latitude edge of the auroral oval. Geomagnetic *H* component at Kaktovik, which is close to the traced point of wave "A," is shown in Figure 4e. In this magnetogram, geomagnetic perturbations which indicate enhancement of electric current fluctuations above Kaktovik appear during 00–02 UT. These results suggest that the electric current in the auroral oval equatorward edge produced the observed AGWs.

[26] The ray tracing analysis mentioned above, however, has a problem. Nonlinear and viscous dissipation effects which increase with height in the thermosphere are not considered. To investigate MSTID behavior and energy flux in more detail, a new AGW propagation theory including the nonlinear and viscous dissipation effects is necessary. This is a future challenge.

[27] The frequency of occurrence and the southwestward propagation of the MSTIDs seem to be determined by the filtering effect and wave source (auroral oval) orientation. This means that the frequency of occurrence and propagation direction of MSTIDs in the Alaskan sector are expected

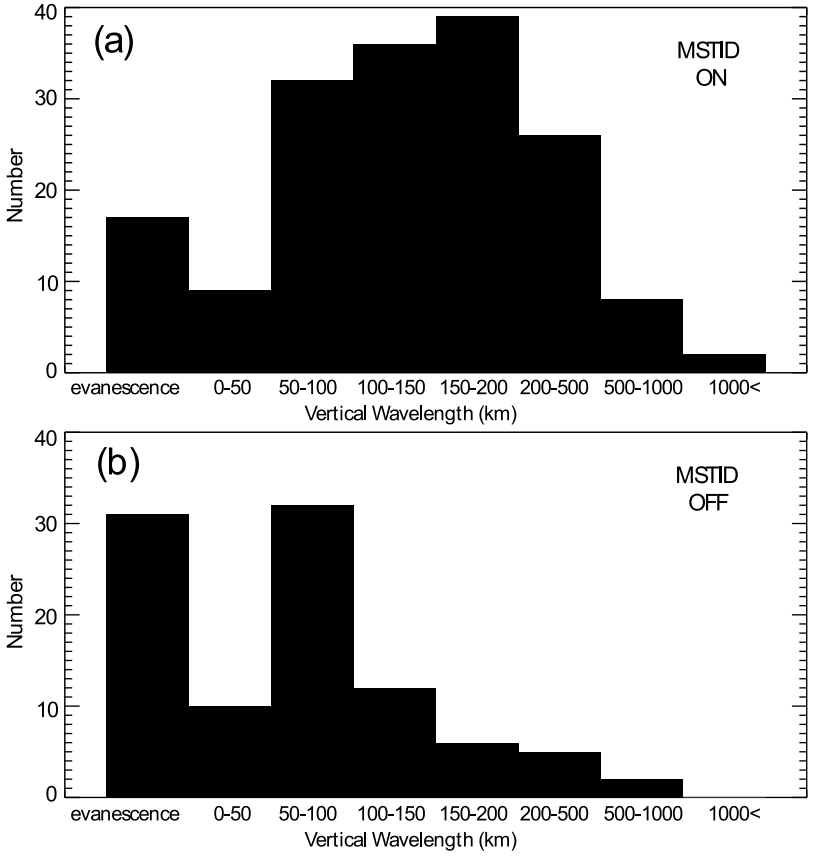

Figure 10. Histograms of vertical wavelengths during November 2001 to April 2002 (a) when MSTIDs appear (on) and (b) when they are not observed (off).

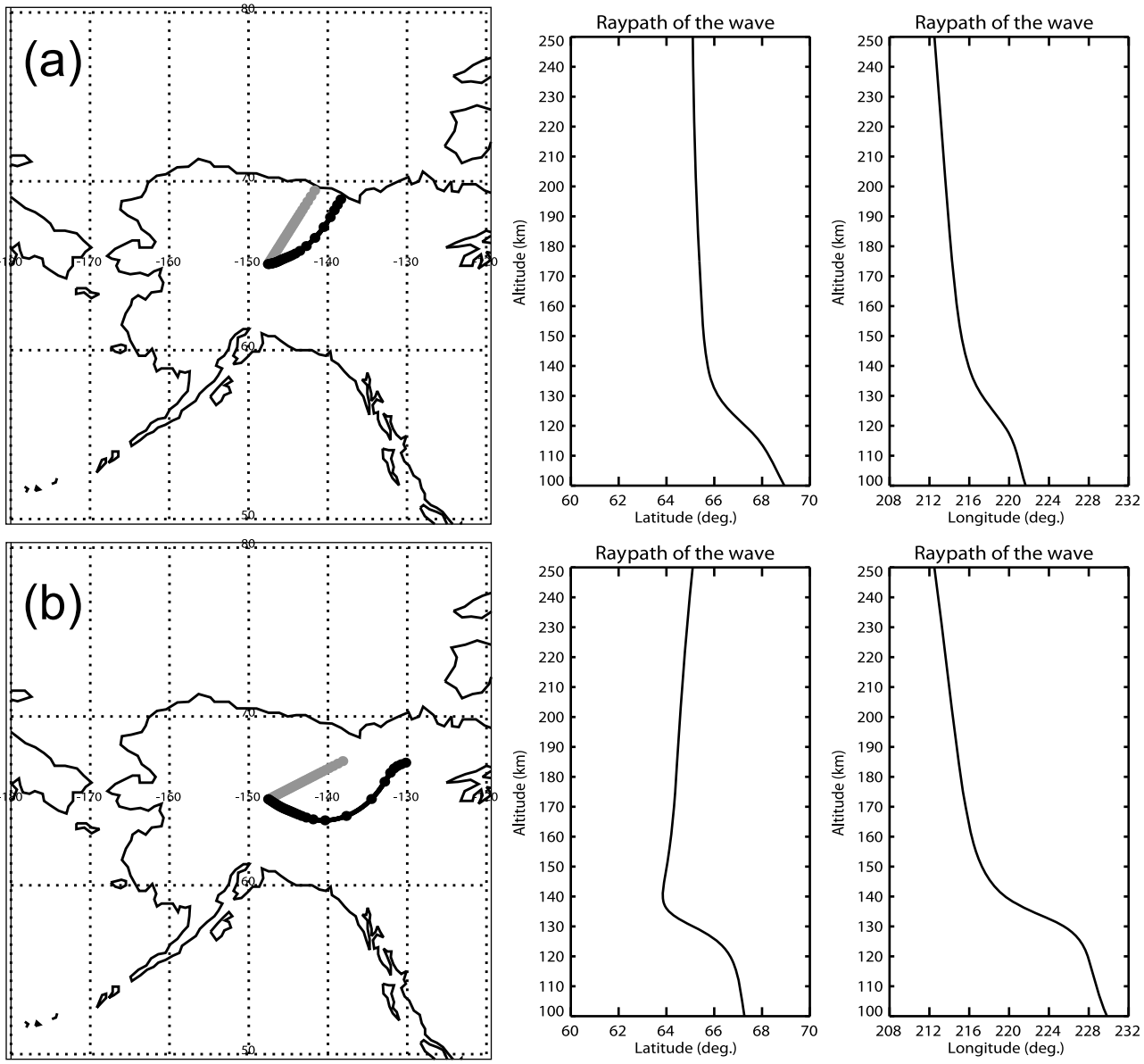

Figure 11. Results of the backward ray tracing analysis applied to (a) the MSTID "A" indicated by the black dashed line in Figure 3 and (b) the MSTID "B" indicated by the white dashed lines in Figure 3. (left) The raypaths of the MSTIDs in a horizontal map. The thick black lines indicate the AGW backward trajectories calculated using the MSIS and HWM models. Gray lines indicate trajectories calculated with an assumption of no wind. (middle and right) The raypaths in the meridian distance-altitude sections and zonal distance-altitude sections, respectively.

to be different from those in the European sector, because the inclination of the auroral oval against the geographic coordinate and background wind field differ between the two locations.

[28] It is well known that AGWs or TIDs are often observed during the day by SuperDARN [*Bristow et al.*, 1996]. *Prikryl et al.* [2005] investigated the source of MSTIDs observed by SuperDARN, and suggested pulsed ionospheric flows near the cusp region as one possible source. In this study, we showed that the MSTIDs observed almost every day in the evening come from the auroral oval. This result suggests that AGWs are continuously generated in the auroral oval. The MSTIDs transport momentum flux from *E* region to *F* region and change the atmospheric wind field when they are dissipated. Thus the MSTIDs play a significant role in the thermosphere and may affect the thermospheric wind field. It is very important to investigate MSTID features in another longitudinal region and in the southern hemisphere.

5. Conclusion

[29] We investigated the characteristics of the MSTIDs frequently observed by our ASI in Alaska.

[30] 1. MSTIDs were observed almost every evening, and sometimes in the morning, but were not observed late at night.

[31] 2. The occurrence of MSTIDs during geomagnetic quiet nights is about 67%. Especially in the evening, the occurrence rate is around 100%. Their propagation direction is mostly southwestward.

[32] 3. The relationships of the MSTID features to the background neutral wind and electric field indicate that MSTIDs are caused by the atmospheric gravity wave, rather than plasma instability.

[33] 4. The results of backward ray tracing analysis suggest that AGWs are generated around the lower-latitude edge of the auroral oval.

[34] 5. The high occurrence rate of MSTIDs indicates that AGWs are continuously generated in the auroral oval and transport momentum flux from the *E* region to *F* region. There is a possibility that these AGWs are affecting the thermospheric wind field.

[35] **Acknowledgments.** The authors would like to thank Brian Lawson at the University of Alaska Fairbanks for his support in the ASI operation at PFRR. Magnetometers at PFRR and Kaktovik are operated by the Geophysical Institute, University of Alaska Fairbanks. The NICT ASIs were developed as a part of the Alaska Project, an international cooperative research project between National Institute of Information and Communications Technology and the University of Alaska Fairbanks. The authors are grateful to the reviewers of this paper for their patient review and helpful comments.

[36] Robert Lysak thanks the reviewers for their assistance in evaluating this paper.

References

Barbier, D. (1959), Recherches sur la raie 6300 de la luminescence atmospherique nocturne, *Ann. Geofis.*, *15*, 179–217.

Barbier, D., and J. Glaume (1962), La couche ionosphérique nocturne *F* dans la zone intertropicale et ses relations avec l'émission de la raie 6300 Å du ciel nocturne, *Planet. Space Sci.*, *9*, 133–148, doi:10.1016/0032-0633(62)90001-6.

Bristow, W. A., R. A. Greenwald, and J. P. Villain (1996), On the seasonal dependence of medium-scale atmospheric gravity waves in the upper atmosphere at high latitudes, *J. Geophys. Res.*, *101*, 15,685–15,699, doi:10.1029/96JA01010.

Conde, M., and R. W. Smith (1997), Phase compensation of a separation scanned, all-sky imaging Fabry-Perot spectrometer for auroral studies, *Appl. Opt.*, *36*, 5441–5450, doi:10.1364/AO.36.005441.

Conde, M., and R. W. Smith (1998), Spatial structure in the thermospheric horizontal wind above Poker Flat, Alaska, during solar minimum, *J. Geophys. Res.*, *103*, 9449–9471, doi:10.1029/97JA03331.

Francis, S. H. (1974), A theory of medium-scale traveling ionospheric disturbances, *J. Geophys. Res.*, *79*, 5245–5260.

Hedin, A. E. (1991), Extension of the MSIS thermospheric model into the middle and lower atmosphere, *J. Geophys. Res.*, *96*, 1159–1172, doi:10.1029/90JA02125.

Hedin, A. E., et al. (1996), Empirical wind model for the upper, middle and lower atmosphere, *J. Atmos. Terr. Phys.*, *58*, 1421–1447, doi:10.1016/0021-9169(95)00122-0.

Hooke, W. H. (1968), Ionospheric irregularities produced by internal atmospheric gravity waves, *J. Atmos. Terr. Phys.*, *30*, 795–823, doi:10.1016/S0021-9169(68)80033-9.

Hooke, W. H. (1970), The ionospheric response to internal gravity waves: 1. The *F* region response, *J. Geophys. Res.*, *75*, 5535–5544, doi:10.1029/JA075i028p05535.

Huang, C. S., C. A. Miller, and M. C. Kelley (1994), Basic properties and gravity-wave initiation of the midlatitude *F*-region instability, *Radio Sci.*, *29*, 395–405, doi:10.1029/93RS01669.

Hunsucker, R. D. (1982), Atmospheric gravity waves generated in the high-latitude ionosphere: A review, *Rev. Geophys.*, *20*(2), 293–315, doi:10.1029/RG020i002p00293.

Kotake, N., Y. Otsuka, T. Ogawa, T. Tsugawa, and A. Saito (2007), Statistical study of medium-scale traveling ionospheric disturbances observed with the GPS networks in Southern California, *Earth Planets Space*, *59*, 95–102.

Kubota, M., et al. (2000), Tracking of wave-like structures in the OI 630 nm nightglow over Japan using an all-sky imagers network during FRONT campaign, *Geophys. Res. Lett.*, *27*, 4037–4040, doi:10.1029/2000GL011858.

Kubota, M., H. Fukunishi, and S. Okano (2001), Characteristics of medium- and large-scale TIDs over Japan derived from OI 630-nm nightglow observation, *Earth Planets Space*, *53*, 741–751.

Kubota, M., S.-I. Oyama, M. Ishii, and Y. Murayama (2002), Recent results and future plans of atmospheric study using CRL all-sky imagers, *J. Commun. Res. Lab.*, *49*, 161–171.

Kubota, M., T. Nagatsuma, and Y. Murayama (2003), Evening co-rotating patches: A new type aurora observed by high sensitivity all-sky cameras in Alaska, *Geophys. Res. Lett.*, *30*(12), 1612, doi:10.1029/2002GL016652.

Kubota, M., et al. (2006), A fast-propagating, large-scale atmospheric gravity wave observed in the WAVE2004 campaign, *J. Geophys. Res.*, *111*, D21110, doi:10.1029/2005JD006788.

Marks, C. J., and S. D. Eckermann (1995), A three-dimensional nonhydrostatic ray-tracing model for gravity waves: Formulation and preliminary results for the middle atmosphere, *J. Atmos. Sci.*, *52*, 1,959–1,984.

Otsuka, Y., K. Shiokawa, T. Ogawa, and P. Wilkinson (2004), Geomagnetic conjugate observations of medium-scale traveling ionospheric disturbances at midlatitude using all-sky airglow imagers, *Geophys. Res. Lett.*, *31*, L15803, doi:10.1029/2004GL020262.

Oyama, S., M. Ishii, Y. Murayama, H. Shinagawa, S. C. Buchert, S. Nozawa, R. Fujii, and W. Kofman (2001), Generation of atmospheric gravity waves associated with auroral activity in the polar *F* region, *J. Geophys. Res.*, *106*, 18,543–18,554, doi:10.1029/2001JA900032.

Oyama, S.-I., Y. Murayama, M. Ishii, and M. Kubota (2002), Development of SALMON system and the environment data transfer experiment, *J. Commun. Res. Lab.*, *49*, 253–257.

Perkins, F. (1973), Spread *F* and ionospheric currents, *J. Geophys. Res.*, *78*, 218–226, doi:10.1029/JA078i001p00218.

Prikryl, P., D. B. Muldrew, G. J. Sofko, and J. M. Ruohoniemi (2005), Solar wind Alfven waves: A source of pulsed ionospheric convection and atmospheric gravity waves, *Ann. Geophys.*, *23*, 401–417, doi:10.5194/angeo-23-401-2005.

Saito, A., S. Fukao, and S. Miyazaki (1998), High resolution mapping of TEC perturbations with the GSI GPS network over Japan, *Geophys. Res. Lett.*, *25*, 3079–3082, doi:10.1029/98GL52361.

Samson, J. C., R. A. Greenwald, J. M. Ruohoniemi, and K. B. Baker (1989), High-frequency radar observations of atmospheric gravity-waves in the high-latitude ionosphere, *Geophys. Res. Lett.*, *16*, 875–878, doi:10.1029/GL016i008p00875.

Shiokawa, K., C. Ihara, Y. Otsuka, and T. Ogawa (2003a), Statistical study of nighttime medium-scale traveling ionospheric disturbances using midlatitude airglow images, *J. Geophys. Res.*, *108*(A1), 1052, doi:10.1029/2002JA009491.

Shiokawa, K., Y. Otsuka, C. Ihara, T. Ogawa, and F. J. Rich (2003b), Ground and satellite observations of nighttime medium-scale traveling ionospheric disturbance at midlatitude, *J. Geophys. Res.*, *108*(A4), 1145, doi:10.1029/2002JA009639.

Yamamoto, M., M. Kubota, S. Takeshita, M. Ishii, Y. Murayama, and M. Ejiri (2002), Calibration of CRL all-sky imagers using an integrating sphere, *Adv. Polar Upper Atmos. Res.*, *16*, 173–180.

M. Conde, Geophysical Institute, University of Alaska Fairbanks, Fairbanks, AK 99775, USA.

M. Ishii, H. Jin, M. Kubota, and Y. Murayama, National Institute of Information and Communications Technology, 4-2-1 Nukui-Kitamachi, Tokyo 184-8795, Japan. (mkubota@nict.go.jp)